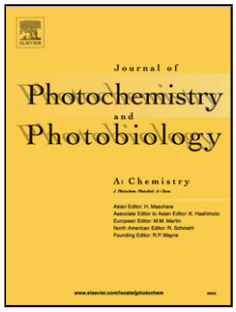

Title: Remarkable difference between five- and six-number-membered ring transition states for intramolecular proton transfer in excited state

Authors: Xiaozhuan Qin, Ge Ding, Zhenqiang Wang, Shengtao Zhang, Hongru Li, Ziping Luo, Fang Gao

PII: S1010-6030(16)31141-8
DOI: http://dx.doi.org/doi:10.1016/j.jphotochem.2017.02.016
Reference: JPC 10542

To appear in: *Journal of Photochemistry and Photobiology A: Chemistry*

Received date: 29-11-2016
Revised date: 14-2-2017
Accepted date: 19-2-2017

Please cite this article as: Xiaozhuan Qin, Ge Ding, Zhenqiang Wang, Shengtao Zhang, Hongru Li, Ziping Luo, Fang Gao, Remarkable difference between five- and six- number-membered ring transition states for intramolecular proton transfer in excited state, Journal of Photochemistry and Photobiology A: Chemistry http://dx.doi.org/10.1016/j.jphotochem.2017.02.016

Remarkable difference between five- and six- number-membered ring transition states for intramolecular proton transfer in excited state

Xiaozhuan Qin[1, 2], Ge Ding[1], Zhenqiang Wang[1], Shengtao Zhang[1], Hongru Li[1*], Ziping Luo[1*], Fang Gao[1*]

[1]College of Chemistry and Chemical Engineering, Chongqing University, Chongqing 400044, China

[2]College of Chemical and Food Engineering, Zhengzhou Institute of Technology, Zhengzhou, Hennan, 450044, China,

Tel/Fax, 86-23-65102531, Emails, hongruli1972@gmail.com, zpluo@126.com, fanggao1971@gmail.com

Graphic Abstract

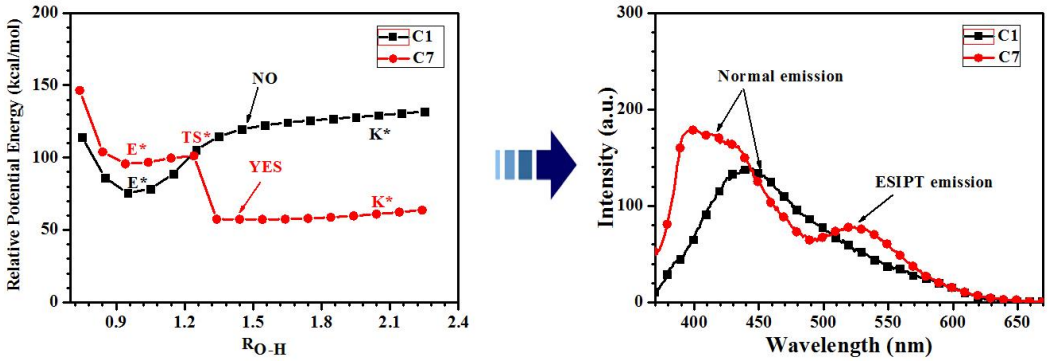

Highlights

- Preparation of dyes with different ring transition states for ESIPT
- Demonstration of different strength internal hydrogen bond in dyes
- Evidence for occurrence or no occurrence of ESIPT of dyes
- Remarkable different potential energy barriers of ESIPT of dyes

Abstract

In this study, a range of organic dyes were prepared to investigate difference between five- and six-number-membered ring transition states for internal proton transfer in excited state. Different strength intramolecular hydrogen bond in the target dyes was demonstrated by X-ray crystallography, ^{1}H-NMR spectroscopy and ultraviolet/visible spectroscopy. The fluorescence measurement suggested excited state intramolecular proton transfer occurred via six number-membered ring transition state, while it could not occur through five number-membered ring transition state. The molecular geometry optimization of the target dyes further accounted for the difference of internal proton transfer in excited state occurred by five- or six-

number-membered ring transition state.

Keywords: Ring transition sate; Internal proton transfer; Excited state; Phototautomerization; Molecular geometry optimization

1. Introduction

Amongst photoinduced processes, proton transfer in excited state is of a special interest as fundamental processes for many important biochemical reactions in life and nature such as in DNA and protein [1-4]. Photoinduced proton transfer occurs from one atom to another atom within a single molecular framework, and proton is normally reversibly transferred to the original atom in the end, which is called as excited state intramolecular proton transfer (ESIPT) [5, 6]. To such an organic molecule, this process can produce unique spectroscopic nature including a normal emission band with its absorption and an abnormal emission band without its absorption [7, 8]. Owing to energy loss caused by proton transfer reaction, this abnormal emission band is greatly shifted and characterized by large Stokes shift, which makes ESIPT molecules as advanced materials for various uses such as fluorescence sensors and electronic optical devices [9, 10].

Therefore, synthesis of new ESIPT organic molecules becomes one of main concerns. It is found that organic molecules undergo internal proton transfer in excited state mainly through quasi six number-membered ring transition states [11-13], while there are few successful reports of organic molecules displaying intramolecular proton transfer in excited state via five number-membered ring transitions [14]. This really confuses us because five number-membered ring possesses quite conformation stability in chemistry.

Hence, it is considered that there are certain other factors determining proton transfer process in excited state. For instance, a typical four-level cycle enol-keto ESIPT process (E→E*→K*→K→E, E, enol, K, keto) includes two actual chemical reactions E*-K* and K-E [15]. So, potential energy barrier of internal enol-keto phototautomerization must be small or even barrierless for ESIPT [16]. This means that internal hydrogen bond between proton donor and proton acceptor must be strong enough so that proton transfer tunnel can be shortened. Thus, formation and stability of transition state of internal phototautomerization could be determined by intramolecular hydrogen bond between proton and proton segments, and as a consequence, ESIPT process could be controlled by varying intramolecular hydrogen bond. For example, internal hydrogen bond strength between neighbouring hydroxy and imino groups could play a significant role in an eno-keto intramolecular phototautomerization.

So far, no comprehensive contrastive study of intramolecular phototautomerization in organic dyes through five- or six- number-membered ring transition state has been carried out. It is necessary to deal with this bewildering scientific question because it would guide us to prepare new organic dyes with ESIPT nature, which leads to an efficient production of dual-emission bands of target organic chromophores.

In this study, we attempt to reveal crucial contributing factors influencing intramolecular phototautomerziation through five- and six- number-membered ring transition states. For this purpose, a variety of enol-keto type target dyes carrying similar chemical structure which provides diversities of transition states for intramolecular proton transfer in excited state are synthesized. We conduct combinational experimental and theoretical investigations to analyze effect of internal hydrogen bond as well as potential energy barrier on occurrence of ESIPT of the target dyes. To

our best knowledge, this is the first successful attempt to find out remarkable difference between five- and six- number-membered ring transition states for intramolecular phototautomerization process. This study would be beneficial for design and synthesis of new ESIPT organic chromophores based on efficient molecule preconstruction.

2. Experimental

2.1. Reagents and characterization

The organic solvents that were further processed by the standard laboratory method were purchased from Aldrich Chemical Corporation [17]. The target organic dyes **C1-C12** were prepared in our own laboratory (**Scheme 1**), which have been reported elsewhere [18]. The melting points of the studied molecules were determined by a Beijing Fukai melting point apparatus, China. ^{1}H and ^{13}C nuclear magnetic resonance (NMR) spectra were measured by Bruke apparatus (400 MHz, 500MHz and 600 MHz) in standard NMR tubes by using tetramethylsilane (TMS) as an internal reference at 25 °C. A CE440 elemental analysis meter from Exeter Analytical Inc. was utilized to perform elemental analysis of the target molecules. Fourier transform infrared spectra of the samples were acquired by KBr pellet method with Nicolet 550II IR spectrometer (Nicolet Instrument Corporation, USA). A UPLC-Q-ToF MS spectrometer (Waters, USA) was utilized to record high resolution mass spectra (HRMS) under electro spray ionization (ESI).

A suitable single crystal of the target molecule that was obtained by slow volatilization of organic solvents in NMR tubes was put inside a glass fiber capillary for measuring molecular structure analyzed by direct methods and refined by full-matrix least squares on F^2. XRD data were collected on a Bruker-AXS CCD area detector equipped with diffractometer with Mo Ka

(λ=0.71073 Å) at 298 K. All the hydrogen atoms were introduced in the calculated positions respectively and all the non-hydrogen atoms were advanced by anisotropic temperature factors.

2.2. Steady and transient Ultraviolet/visible and fluorescence spectroscopic determination

Spectral grade organic solvents were utilized to the spectroscopic measurement. A TU1901 spectrophotometer from Beijing PUXI General Equipment Limited Corporation was used to measure ultraviolet/visible (UV/visible) absorption spectra of the samples. The fluorescence emission spectra of the samples were recorded by Shimadzu RF-531PC spectrofluorophotonmeter. Quinine sulfate in 0.5 mol/L H_2SO_4 (Φ, 0.546) was used as the reference to determine fluorescence quantum yields of the studied dyes [19]. The absorption at the excited wavelength is below 0.1 for removal of the experimental errors of fluorescence quantum yields.

The fluorescence lifetimes of the samples were measured by a ultrafast laser system. Time-resolved laser measurement was performed through a spectrograph using a connected intensified double photodiode array. The pulses were focused onto a sample cuvette containing 100 μm thick fused-silica window and a 250 pm optical path length. The transient emission spectra were recorded by a ultrafast white-light continuum.

2.3. Molecular geometry optimization computation

Molecular geometry computation of the target molecules was carried out by 6-31G** basis set in Gaussian 09 program package. The phototautomers enol and keto geometry optimization in ground state (S_0) was performed by using B3LYP method on basis of Hartree-Fock (HF) level [20], while single-excitation configuration interaction (CIS) was employed to optimize the geometries

in the first singlet excited state (S_1). The energies of optimized geometries of S_0 and S_1 states were computed by density functional theory (DFT) and time-dependence DFT (TD-DFT) method at HF and CIS levels respectively such as DFT//HF or TDDFT//CIS (the single-point calculation//optimization method) [21]. The organic solvents were used as the media for theoretical computation.

2.4. Synthesis of the target dyes

The synthesis approaches of the target dyes are depicted in **Scheme 1**. The preparation procedure and chemical structural characterization of the studied dyes are described in the followings.

2.4.1. General procedure for carbonylation of o-hydroxyaniline and o-methoxyaniline derivatives

A solution of 6 mmol of the corresponding aldehyde and 5 mmol of o-hydroxyaniline or o-methoxyaniline in 30 mL of anhydrous ethanol was stirred at 25 °C for 24 h. The target dyes could be further purified by silicon gel column chromatography and recrystallization.

C1, 2-(benzylideneamino)-phenol White solid (yield, 91%), m.p., 89.5-90.1 °C. ^{1}H-NMR (500 MHz, DMSO-d_6) δ (ppm): 9.010 (s, Ar-OH, 1H), 8.712 (s, N=CH, 1H), 8.046-8.027 (m, Ar-H, 2H), 7.530-7.508 (m, Ar-H, 3H), 7.219-7.200 (m, Ar-H, 1H), 7.109-7.075 (m, Ar-H, 1H), 6.920-6.904 (t, J = 8 Hz, Ar-H, 1H), 6.863-6.832 (t, J = 7.8 Hz, Ar-H, 1H). ^{13}C-NMR (151 MHz, DMSO-d_6) δ (ppm): 161.285, 156.165, 145.241, 137.164, 131.329, 130.476, 129.382, 128.864, 126.613, 124.246, 122.463, 118.183, 114.519. IR (KBr, cm^{-1}): 3374.6, 3326.6, 2915.0, 1625.1,

1482.5, 1381.0, 1250.9, 1195.2, 850.9, 765.8, 689.5, 646.1, 502.5. Elementary analysis, Anal. Calcd for $C_{13}H_{11}NO$, C, 79.16, H, 5.62, N, 7.10; Found, C, 79.24, H, 5.55, N, 7.23. HRMS (ESI) m/z: calcd for $C_{15}H_{16}N_2O$ $[M+H]^+$ 198.0914, found, 198.0918.

C2, 2-(4-methoxybenzylideneamino)-phenol White solid (yield, 88%), m.p., 86.5-87.5 °C. ^{1}H-NMR (500 MHz, DMSO-d_6) δ (ppm): 8.885 (s, Ar-OH, 1H), 8.615 (s, N=CH, 1H), 7.987-7.970 (d, J = 8.5 Hz, Ar-H, H), 7.177-7.158 (m, Ar-H, 1H), 7.068-7.035 (m, Ar-H, 3H), 6.889-6.873 (t, J = 8 Hz, Ar-H, 1H), 6.835-6.805 (t, J = 15 Hz, Ar-H, 3H), 3.835 (s, Ar-OMe, 3H). ^{13}C-NMR (151 MHz, DMSO-d_6) δ (ppm): 161.999, 159.842, 151.586, 140.973, 133.028, 131.016, 129.125, 128.874, 122.876, 119.987, 114.562, 113.218, 112.563, 56.087. IR (KBr, cm^{-1}): 3341.8, 3016.2, 2836.1, 1595.5, 1486.5, 1422.6, 1258.4, 1168.0, 1028.0, 833.7, 756.4, 643.3. Elementary analysis, Anal. Calcd for $C_{14}H_{13}NO_2$, C, 73.99, H, 5.77, N, 6.16; Found, C, 74.15, H, 5.8, N, 6.25. HRMS (ESI) m/z: calcd for $C_{14}H_{13}NO_2$ $[M+H]^+$ 228.1019, found, 228.1021.

C3, 2-(4-cyanobenzylideneamino)-phenol Pale yellow solid (yield, 82%), m.p., 133.5-134.5 °C. ^{1}H-NMR (500 MHz, DMSO-d_6) δ (ppm): 9.191 (s, Ar-OH, 1H), 8.842 (s, N=CH, 1H), 8.239-8.223 (d, J = 8 Hz, Ar-H, 2H), 7.996-7.980 (d, J = 8 Hz, Ar-H, 2H), 7.298-7.280 (m, Ar-H, 1H), 7.156-7.122 (m, Ar-H, 1H), 6.935-6.850 (m, Ar-H, 2H). ^{13}C-NMR (151 MHz, DMSO-d_6) δ (ppm): 159.917, 152.554, 141.762, 133.245, 131.297, 129.092, 128.341, 127.654, 125.971, 123.041, 120.091, 118.814, 118.782, 115,782. IR (KBr, cm^{-1}): 3398.5, 2222.9, 1625.3, 1567.0, 1484.5, 1380.6, 1256.6, 1149.7, 950.5, 833.2, 747.7, 626.8, 547.5. Elementary analysis, Anal. Calcd for $C_{14}H_{10}N_2O$, C, 75.66, H, 4.54, N, 12.60; Found, C, 75.73, H, 4.33, N, 12.72. HRMS (ESI) m/z: calcd for $C_{14}H_{10}N_2O$ $[M+H]^+$ 223.0866, found, 223.0869.

C4, 2-methoxy-*N*-(benzylidene)-aniline White solid (yield, 87%), m.p., 82.9-84.9 °C.

^{1}H-NMR (400 MHz, DMSO-d_6) δ (ppm): 8.619 (s, N=CH, 1H), 7.908-7.886 (m, Ar-H, 2H), 7.495-7.480 (t, J = 6 Hz, Ar-H, 3H), 7.293-7.271 (d, J = 8.8 Hz, Ar-H, 2H), 6.977-6.955 (d, J = 8.8 Hz, Ar-H, 2H), 3.761 (s, Ar-OMe, 3H). ^{13}C-NMR (151 MHz, DMSO-d_6) δ (ppm): 159.867, 153.682, 145.638, 141.457, 138.827, 134.396, 132.196, 129.782, 128.372, 124.682, 121.187, 117.291, 116.652, 56.824. IR (KBr, cm^{-1}): 1637.2, 1618.3, 1508.3, 1400.4, 1248.6, 1026.5, 739.5, 616.3, 474.6. Elementary analysis, Anal. Calcd for $C_{14}H_{13}NO$, C, 79.59, H, 6.20, N, 6.63; Found, C, 79.67, H, 6.11, N, 6.75. HRMS (ESI) m/z: calcd for $C_{14}H_{13}NO$ $[M+H]^+$ 212.107, found, 212.1077.

C5, 2-methoxy-*N*-(4-methoxybenzylidene)-aniline White solid (yield, 93%), m.p., 48.6-50.1 °C. ^{1}H-NMR (400 MHz, DMSO-d_6) δ (ppm): 8.398 (s, N=CH, 1H), 7.853-7.833 (d, J = 8 Hz, Ar-H, 2H), 7.160-7.123 (m, Ar-H, 1H), 7.057-6.909 (m, Ar-H, 5H), 3.818 (s, Ar-OMe, 3H), 3.763 (s, Ar-OMe, 3H). ^{13}C-NMR (151 MHz, DMSO-d_6) δ (ppm): 161.231, 159.005, 153.512, 139.126, 132.536, 131.001, 129.874, 126.472, 125.489, 121.016, 115.305, 114.652, 113.987, 56.071, 55.628. IR (KBr, cm^{-1}): 2836.3, 1683.0, 1604.3, 1511.2, 1462.9, 1263.8, 1162.9, 1027.7, 833.8, 746.2, 642.2, 607.4, 518.4. Elementary analysis, Anal. Calcd for $C_{15}H_{15}NO_2$, C, 74.67, H, 6.27, N, 5.81; Found, C, 74.73, H, 6.14, N, 5.90. HRMS (ESI) m/z: calcd for $C_{15}H_{15}NO_2$ $[M+H]^+$ 242.1176, found, 242.1181.

C6, 2-methoxy-*N*-(4-cyanobenzylidene)-aniline Pale yellow solid (yield, 88%), m.p., 73.1-74.3 °C. ^{1}H-NMR (400 MHz, DMSO-d_6) δ (ppm): 8.642 (s, N=CH, 1H), 8.080-7.957 (m, Ar-H, 4H), 7.211 (s, Ar-H, 1H), 7.095-7.064 (t, Ar-H , J = 12.4 Hz, 2H), 6.969 (s, Ar-H, 1H), 3.792 (s, Ar-OMe, 3H). ^{13}C-NMR (151 MHz, DMSO-d_6) δ (ppm): 160.152, 153.016, 141.231, 140.862, 139.982, 133.627, 131.267, 127.241, 123.561, 121.735, 119.874, 116.724, 115.421,

114.992, 55.876. IR (KBr, cm^{-1}): 2834.6, 2225.2, 1637.8, 1582.1, 1493.3, 1434.8, 1250.0, 1171.2, 1112.9, 1022.6, 977.6, 861.1, 831.5, 781.5, 757.0, 568.2, 535.7. Elementary analysis, Anal. Calcd for $C_{15}H_{12}N_2O$, C, 76.25, H, 5.12, N, 11.86; Found, C, 76.31, H, 5.22, N, 11.97. HRMS (ESI) m/z: calcd for $C_{15}H_{12}N_2O$ $[M+H]^+$ 237.1023, found, 237.1030.

2.4.2. General procedure for amination of salicylaldehyde and o-methoxybenzaldehyde derivatives

A solution of 6 mmol of the corresponding amine and 5 mmol of salicylaldehyde or o-methoxybenzaldehyde in 30 mL of anhydrous ethanol was stirred at 25 ℃ for 24 h. The target molecules could be further purified by silicon gel column chromatography as well as recrystallization.

C7, 2-((phenylimino)methyl)-phenol White solid (yield, 86%), m.p., 50-51°C. ^{1}H-NMR (600 MHz, DMSO-d_6) δ (ppm): 13.074 (s, Ar-OH, 1H), 8.941 (s, N=CH, 1H), 7.651-7.638 (d, J = 7.8 Hz, Ar-H, 1H), 7.463-7.389 (m, Ar-H, 5H), 7.312-7.287 (t, J = 7.5 Hz, Ar-H, 1H), 6.981-6.945 (m, Ar-H, 2H). ^{13}C-NMR (151 MHz, DMSO-d_6) δ (ppm): 161.009, 159.651, 153.981, 136.238, 135.016, 134.365, 130.094, 127.859, 125.372, 123.253, 121.587, 121.274, 118.372. IR (KBr, cm^{-1}): 3414.0, 2884.1, 1616.2, 1571.6, 1483.8, 1455.3, 1400.8, 1359.1, 1276.6, 1186.7, 1150.0, 1074.5, 981.2, 867.0, 845.4, 755.7, 692.4, 547.8. Elementary analysis, Anal. Calcd for $C_{13}H_{11}NO$, C, 79.16, H, 5.62, N, 7.10; Found, C, 79.27, H, 5.55, N, 7.23. HRMS (ESI) m/z: calcd for $C_{13}H_{11}NO$ $[M+H]^+$ 198.0914, found, 198.0909.

C8, 2-((4-methoxyphenylimino)methyl)-phenol White solid (yield, 89%), m.p., 71.5-72.3 ℃. ^{1}H-NMR (600 MHz, DMSO-d_6) δ (ppm): 13.263 (s, Ar-OH, 1H), 8.910 (s, N=CH, 1H),

7.592-7.579 (d, *J* = 7.8 Hz, Ar-H, 1H), 7.402-7.345 (m, Ar-H, 3H), 7.002-6.987 (d, *J* = 9 Hz, Ar-H, 2H), 6.951-6.910 (m, Ar-H, 2H), 3.776 (s, Ar-OMe, 3H). ^{13}C-NMR (151 MHz, DMSO-d_6) δ (ppm): 161.005, 160.997, 159.874, 144.537, 135.379, 133.024, 123.069, 122.106, 121.058, 120.145, 118.762, 116.594, 115.617, 55.078. IR (KBr, cm^{-1}): 3411.2, 2964.3, 2841.7, 1621.2, 1571.1, 1509.7, 1492.3, 1406.0, 1276.5, 1247.8, 1187.9, 1033.6, 983.2, 910.5, 838.7, 748.6, 632.0, 545.4. Elementary analysis, Anal. Calcd for $C_{14}H_{13}NO_2$, C, 73.99, H, 5.77, N, 6.16; Found, C, 74.13, H, 5.63, N, 6.27. HRMS (ESI) m/z: calcd for $C_{14}H_{13}NO_2$ $[M+H]^+$ 228.1019, found, 228.1026.

C9, 2-((4-cyanophenylimino)methyl)-phenol Pale yellow solid (yield, 80%), m.p., 83.5-84.5 °C. ^{1}H-NMR (600 MHz, DMSO-d_6) δ (ppm): 12.386 (s, Ar-OH, 1H), 8.933 (s, N=CH, 1H), 7.894-7.880 (d, *J* = 8.4 Hz, Ar-H, 2H), 7.681-7.668 (d, *J* = 7.8 Hz, Ar-H, 1H), 7.528-7.514 (d, *J* = 8.4 Hz, Ar-H, 2H), 7.441-7.415 (t, *J* = 7.8 Hz, Ar-H, 1H), 6.983-6.952 (t, *J* = 9 Hz, Ar-H, 2H) . ^{13}C-NMR (151 MHz, DMSO-d_6) δ (ppm): 163.065, 157.063, 151.983, 135.682, 134.013, 132.673, 131.786, 124.035, 125.484, 122.531, 121.087, 119.643, 117.835, 111.153. IR (KBr, cm^{-1}): 3416.8, 3067.7, 2981.8, 2227.4, 1616.6, 1565.0, 1503.8, 1454.0, 1393.8, 1359.7, 1273.9, 1172.7, 1150.1, 1031.5, 972.6, 908.1, 858.5, 823.5, 760.5, 622.8, 558.9, 543.3. Elementary analysis, Anal. Calcd for $C_{14}H_{10}N_2O$, C, 75.66, H, 4.54, N, 12.60; Found, C, 75.71, H, 4.48, N, 12.73. HRMS (ESI) m/z: calcd for $C_{14}H_{10}N_2O$ $[M+H]^+$ 223.0866, found, 223.0872.

C10, *N*-(2-methoxybenzylidene)-aniline Pale yellow solid (yield, 90%), m.p., 41-42 °C. ^{1}H-NMR (600 MHz, DMSO-d_6) δ (ppm): 8.816 (s, N=CH, 1H), 8.005-7.989 (d, *J* = 9.6 Hz, Ar-H, 1H), 7.519-7.493 (t, *J* =7.8 Hz, Ar-H, 1H), 7.399-7.373 (t, *J* = 7.8 Hz, Ar-H, 2H), 7.218-7.137 (m, Ar-H, 4H), 7.058-7.033 (t, *J* = 7.5 Hz, Ar-H, 1H), 3.869 (s, Ar-OMe, 3H). ^{13}C-NMR (151 MHz,

DMSO-d_6) δ (ppm): 157.764, 153.268, 139.167, 133.254, 131.215, 130.261, 128.574, 127.563, 125.346, 123.365, 122.915, 119.821, 112.326, 56.091. IR (KBr, cm^{-1}): 2836.8, 1616.8, 1586.0, 1489.2, 1467.7, 1363.6, 1264.7, 1252.6, 1187.4, 1159.6, 1105.6, 1045.6, 1021.6, 970.2, 880.7, 758.3, 690.9, 516.6. Elementary analysis, Anal. Calcd for $C_{14}H_{13}NO$, C, 79.59, H, 6.20, N, 6.63; Found, C, 79.65, H, 6.13, N, 6.75. HRMS (ESI) m/z: calcd for $C_{14}H_{13}NO$ $[M+H]^+$212.107, found, 212.1062.

C11, 4-methoxy-*N*-(2-methoxybenzylidene)-aniline White solid (yield, 91%), m.p., 58.6-59.1 °C. ^{1}H-NMR (600 MHz, DMSO-d_6) δ (ppm): 8.867 (s, N=CH, 1H), 7.784-7.778 (d, *J* = 3.6 Hz, Ar-H, 1H), 7.591-7.577 (d, *J* = 8.4 Hz, Ar-H, 2H), 7.389-7.334 (m, Ar-H, 4H), 7.276-7.247 (t, *J* = 9 Hz, Ar-H, 1H), 3.872 (s, Ar-OMe, 3H), 3.862 (s, Ar-OMe, 3H). ^{13}C-NMR (151 MHz, DMSO-d_6) δ (ppm): 159.876, 157.034 156.983, 145.002, 133.012, 132.615, 128.051, 127.632, 125.174, 123.031, 122.093, 121.168, 116.513, 56.037, 55.318. IR (KBr, cm^{-1}): 2837.9, 1621.7, 1577.0, 1505.9, 1400.3, 1268.2, 1248.4, 1191.7, 1110.5, 1030.2, 957.1, 834.9, 754.7, 616.8, 550.2. Elementary analysis, Anal. Calcd for $C_{15}H_{15}NO_2$, C, 74.67, H, 6.27, N, 5.81; Found, C, 74.71, H, 6.19, N, 5.96. HRMS (ESI) m/z: calcd for $C_{15}H_{15}NO_2$ $[M+H]^+$ 242.1176, found, 242.1183.

C12, 4-cyano-*N*-(2-methoxybenzylidene)-aniline yellow solid (yield, 84%), m.p., 63.1-64.3 °C. ^{1}H-NMR (600 MHz, DMSO-d_6) δ (ppm): 8.859 (s, N=CH, 1H), 8.352-8.331 (d, *J* = 8.4 Hz, Ar-H, 2H), 8.173-8.152 (d, *J* = 8.4 Hz, Ar-H, 2H), 7.351-7.310 (t, *J* = 8.2 Hz, Ar-H, 1H), 6.911-6.848 (m, Ar-H, 3H), 3.855 (s, Ar-OMe, 3H). ^{13}C-NMR (151 MHz, DMSO-d_6) δ (ppm): 157.871, 156.437, 155.653, 133.213, 133.216, 131.086, 127.042, 125.091, 123.146, 122.071, 120.948, 118.456,112.099, 110.097, 55.672. IR (KBr, cm^{-1}): 2227.4, 1608.7, 1560.7, 1345.8,

1214.6, 1108.3, 1027.3, 977.6, 858.1, 781.5, 652.3, 538.2. Elementary analysis, Anal. Calcd for $C_{15}H_{12}N_2O$, C, 76.25, H, 5.12, N, 11.86; Found, C, 76.38, H, 5.06, N, 11.98. HRMS (ESI) m/z: calcd for $C_{15}H_{12}N_2O$ $[M+H]^+$ 237.1023, found, 237.1032.

3. Results and discussion

3.1. The target dyes

In this work, the designed target dyes shown in **Scheme 1** contain a similar proton transfer skeleton as a representative ESIPT molecule salicylidene methylamine [22], which are divided into two groups: (i) the dyes could undergo enol-keto phototautomerizaiton via a five number-membered ring transition state (**C1-C3**), (ii) the dyes could process excited state intramolecular proton transfer via a six number-membered ring transition state (**C7-C9**). The methylated studied dyes are used as the references for comparing spectroscopic properties to those of the target ones. Electron-donating and withdrawing groups are introduced to vary intramolecular hydrogen bond strength of the target dyes, and thus internal proton transfer in excited state could be tuned.

3.2. Intramolecular hydrogen bond based on analysis of ^{1}H-NMR spectra

The higher melting points of the target dyes with respect to those of the corresponding reference dyes indicate the presence of special internal interaction in the target dyes. It is well-accepted that hydrogen bond leads to an increase of ^{1}H-NMR chemical shift of relevant hydrogen atoms, which means a detectable downshift to magnetic field due to the deshielding effect [23]. In order to remove NMR peak interference of deuterated chloroform ($CDCl_3$) and

increase the solubility, DMSO-d_6 was chosen as the deuterated solvent in NMR spectral measurement. In particular, ^{1}H-NMR peak of phenolic hydroxy group in target dyes could be well identified in DMSO-d_6.

The typical ^{1}H-NMR spectra of the target molecules **C1** and **C7** as well as the corresponding reference molecules **C4** and **C10** in DMSO-d_6 are shown in **Figure 1** and **Figure S1** respectively (***Figures S*** and ***Tables S*** *are included in* ***Supplementary Materials***). As shown in **Figure 1**, ^{1}H-NMR chemical shifts of imino groups in the references are located at the higher magnetic field comparing to those in targets (such as **C1**, 8.712 ppm *versus* **C4**, 8.619 ppm, in **Figure S1**). In addition, ^{1}H-NMR chemical shift of CH=N in **C1** or **C4** also switch to the higher magnetic field comparing to those in **C7** or **C10** correspondingly (such as **C1**, 8.712 ppm *versus* **C7**, 8.941 ppm, **Figure 1**). These indicate that there is an intramolecular H-bond between phenolic and imino groups in **C1** and **C7**.

It is remarkable that ^{1}H-NMR chemical shift of phenolic group in **C7** moves to much lower magnetic field comparing to that in **C1** (such as **C1**, 9.010 ppm *versus* **C7**, 13.074 ppm, **Figure 1**), which suggests that there is a stronger intramolecular hydrogen bond between adjacent phenolic hydroxy and imino groups in **C7** than that in **C1**. Hence, it is deduced that formation and stability of six number-membered ring transition state in **C7** are greater than five number-membered ring one in **C1** [24], and as a consequence, ESIPT can be more easily proceeded in **C7**.

The other target dyes show similar nuclear magnetic resonance spectral characteristics. It is further observed that ^{1}H-NMR chemical shift of phenolic group in **C1**-**C3** shifts to more down-magnetic fields with the substitution of electron-accepting groups (**C1**, 9.010 ppm, **C2**, 8.659 ppm, and **C3**, 9.257 ppm). In contrast, phenolic group in **C7**-**C9** moves to lower magnetic

field by substituting electron-donating groups (**C7**, 13.074 ppm, **C8**, 13.263 ppm, **C9**, 12.386 ppm). This means that internal hydrogen bond in the target dyes can be also tuned by varying substituents.

3.3. Intramolecular hydrogen bond based on X-single crystal diffraction analysis

The molecular structures of the target dyes are further confirmed by X-single crystal diffraction analysis. The atomic visualization in single crystal authenticates molecular structures of the target dyes. **Figure 2** shows that there is an intramolecular hydrogen bond between the neighboring phenolic hydroxy and imino groups in **C1** and **C7** respectively. It is given from X-ray single crystal diffraction that the **C1** and **C7** both exist as E isomers of C=N double bond, which offers great coplanarity in **C1** and **C7** respectively.

X-ray single crystal diffraction shows that the distance between phenolic hydrogen and imino groups in **C7** is 1.902 Å, while it is shorter in **C1** (N1-H1, 2.129 Å for **C1**), which demonstrates a stronger intramolecular hydrogen bond in **C7**. The data further suggest that **C1** presents longer N1-O1 (2.616 Å for **C1**, 2.613 Å for **C7**) and larger dihedral angle of ∠C-O1-H1-N1 (∠ C2-O1-H1-N1 for **C1**, -0.79˚; ∠C3-O1-H1-N1 for **C7**, -0.46˚) in phenolic hydroxy and imino groups than **C7**. This further indicates that there is a harder internal hydrogen bond in **C7** comparing to that in **C1**.

X-ray single crystal diffraction suggests that formation of five number-membered ring transition state in **C1** could be more difficult as comparing to that of six number-membered ring one in **C7**. In addition, the stability of five number-membered transition state in **C1** could be weaker than that of six number-membered ring one in **C7**. Hence, it is much possible that the

formation of five number-membered ring transition state in **C1** display higher energy barrier than that of six number-membered one in **C7**. As a consequence, it is more difficult to undergo intramolecular proton transfer through a five number-membered ring transition state in excited state of **C1**.

3.4. Effect of intramolecular hydrogen bond on steady ultraviolet/visible and emission spectra

Ultraviolet/visible spectra of the target and the reference molecules were studied in various organic solvents. The typical UV/visible spectra of the studied dyes in 1,4-dioxane and DMF are given in **Figure 3**, and the representative UV/visible spectral parameters of are presented in **Table 1**. **(**also see **Figure S2** & **Table S1**). It is found that the studied dyes show similar UV/visible shapes in various solvents, while the absorption maxima exhibit variations with electron donor/accepting substituents. This suggests that the long-wavelength peak could be assigned to (π, π^*) transition with intramolecular charge transfer nature due to π-conjugation of entire molecular framework.

It is noticed that the target dyes exhibit a bathochromic shift of the absorption peak wavelength with respect to the methylated reference ones correspondingly (such as in DMF, **C1**, 348 nm, **C4**, 336 nm), although methoxyl group is a stronger electron-donating group. The results indicate that internal hydrogen bond increases intramolecular charge transfer of entire molecules, and the energy of (π, π) transition decreases accordingly.

Therefore, it is considered that intramolecular proton transfer in excited state of these target dyes could occur [25]. The fluorescence emission spectra of the studied dyes were investigated in

various organic solvents to get the direct experimental evidence. The typical fluorescence spectra of the studied dyes in 1,4-dioxane and DMF are depicted in **Figure 4**. The representative fluorescence spectral parameters are provided in **Table 2** (also see **Figure S2** & **Table S1**).

It is found that **C7** exhibits well-separated dual emission bands, while **C10** shows single fluorescence band. In addition, the peak wavelength of the first emission band of **C7** is close to the emission maximum of **C10** with normal Stokes shift (such as in DMF, **C10**, 405 nm, **C7**, 409 nm, Stokes shift, about 4 nm). In contrast, the second emission band of **C7** is remarkably red-shifted and characterized with huge Stokes shift (such as in DMF, **C7**, 517 nm, Stokes shift, about 112 nm). The similar fluorescence emission experimental phenomena are yielded to the partners **C8**/**C11** and **C9**/**C12**. The results show that the first emission band of **C7-C9** is assigned to the normal enol form decay of single excited state, while the second emission band is produced by the excited keto tautomer produced by intramolecular proton transfer in excited state through a six-membered ring transition state (**Scheme 2(a)**).

In contrast, the partners **C1**/**C4**, **C2**/**C5** and **C3**/**C6** show almost identical single emission band shape with normal Stokes shift respectively in various solvents. Hence, the results show that the fluorescence emission of these partners is produced by the normal decay of $S_1 \rightarrow S_0$, which means that **C1-C3** can not undergo internal proton transfer in excited state through a five number-membered ring transition state, and the keto tautomers are not yielded (**Scheme 2(b)**). It is found that there is an emission shoulder of the partner **C3**/**C6** that could be assigned to internal charge transfer due to strong electron-accepting effect of cyano group.

It is also found that the targets **C7-C9** exhibits strong competitive ESIPT emission in solid state or polymer matrix, while the solids **C1-C3** only show normal emission that is almost

identical to the corresponding reference dyes (**Figure S4**). The results further demonstrate that it is more easily to undergo ESIPT through a six number-membered ring transition state than a five number-membered ring one (**Scheme 2**), which could be ascribed to the stronger internal hydrogen bond in **C7**-**C9** comparing to that in **C1**-**C3**. It is also discovered that the emission intensity ratios of keto to enol forms and the wavelengths of keto tautomers of the targets **C7**-**C9** can be tuned by varying the substituents and the media.

3.5. Time-resolved fluorescence emission spectra

Time-resolved fluorescence decay of 2-((phenylimino)methyl)-phenol (**C7**) have ever been reported [26, 27]. So, we performed an investigation of time-dependent fluroescence decay profiles of **C2** and **C8** in this study. It is found that **C2** displays a similar fluorescence lifetime as its methylated reference (**C5**), which is also approximate to the first emission band of **C8** (such as in 1,4-dioxane, **C2**, 2.63×10^{-11} s at 456 nm, **C5**, 2.34×10^{-11} s at 452 nm, **C8**, 2.26×10^{-11} s at 393 nm). It is found that the methylated molecule **C11** also shows the similar fluorescence lifetime (such as in 1,4-dioxane, **C11**, 2.07×10^{-11} s at 392 nm). It is also noticed that the other emission wavelengths of **C2** show almost identical fluorescence lifetime as the maximal emission wavelength.

While in contrast, the second emission band of **C8** exhibits a shorter fluorescence lifetime than the first one in various solvents (such as in 1,4-dioxane, 1.78×10^{-12} s at 504 nm). The results suggest that the fluorescence band of **C2** and the first fluorescence band of **C8** are assigned to the excited enol forms producing typical normal $S_1\rightarrow S_0$ emission decay. However, the excited keto form of **C2** yielded by phototatutomerization could show a more competitive radiative transition

than the excited enol form.

The radiative and non-radiative transition constants (k_r, k_{nr}) in excited state of a dye can be calculated according to the following equations [28-30]:

$k_r = \Phi_f/\tau_f$ (1)

$k_{nr} = (1-\Phi_f)/\tau_f$ (2)

wherein Φ_f shows fluorescence quantum yield of a dye and τ_f represents fluorescence lifetime obtained at the maximal emission wavelength of a dye. Since **C8** yields the enol fluorescence band and the keto fluorescence band, the fluorescence quantum yield of **C8** can be considered as the sum including the normal fluorescence quantum yield and ESIPT fluorescence quantum yield, which can be described as:

$$\Phi_{f\,(sum)} = \Phi_{f\,(enol)} + \Phi_{f\,(keto)} \quad (3)$$

Wherein $\Phi_{f\,(sum)}$ shows the fluorescence quantum yield of the studied dyes, $\Phi_{f\,(enol)}$ represents the fluorescence quantum yield of the enol forms of the studied dyes, $\Phi_{f\,(keto)}$ is the fluorescence quantum yield of the keto forms of the studied dyes.

Because UV/visible absorption of **C2** is produced by tautomer enol to enol*, the integrated area ratio of the enol emission band or the keto emission band to the total emission represents the percent of the normal fluorescence quantum yield or the ESIPT fluorescence quantum yield respectively. As a result, the normal fluorescence quantum yield and ESIPT fluorescence quantum yield of **C8** can be obtained respectively. The radiative and non-radiative transition constants of the tautomers in excited state of **C8** can be calculated.

Radiative and non-radiatibe transition constants of **C2/C5** and **C8/C11** are given in **Table 3**. The data suggest that keto emission band of **C8** show much larger radiative transition constant

than the enol emission band (such as in DMF, **C8**, $k_{r(keto)}$, 1.17×10^{10} s^{-1}, $k_{r(enol)}$, 5.01×10^{9} s^{-1}), which indicates that the excited keto form of **C8** is more competitive in excited state. It is further found that the nonradiative transition rate of **C2** is greater than that of the normal emission band of **C8**, reflecting that internal proton transfer decreases the transition decay of the excited enol form.

Time-dependence transient fluorescence spectra of **C8** registered by decay kinetics basing on dependence of emission wavelength are used to distinguish excited keto form from excited enol tautomer. The peak transient tautomer enol emissive species of **C8** in 1,4-dioxane is yielded at 2.0×10^{-11} s (**Figure 5**). However, its intensity decreases with the decay time course. The peak transient keto band appears at 6.0×10^{-11} s decay time range. It is further found that both of transient species exhibit the diminished emission intensity with decay process. Overall, time-resolved fluorescence emission profiles of **C8** further demonstrate intramolecular proton transfer in excited state. In contrast, only presence of transient tautomer enol emissive peak of **C2** means that internal proton transfer in excited states does not occur (**Figure S5**).

3.6. Molecular geometry optimization

3.6.1. Frontier orbitals, Mulliken atomic charge and dipole moment

Frontier orbitals of excited enol tautomer associating with enol-keto phototautomerization of the target dyes are shown in **Figure 6**. To excited enol form of **C1**, electron cloud density in HOMO is mainly located at *o*-hydroxy-phenyl-imino part, but it shifts to conjugated phenyl ring in LUMO. The absence of electron cloud density distribution in *o*-hydroxy-phenyl-imino part in LUMO of excited enol form indicates that proton transfer part could be inactive in excited enol form of **C1**.

In contrast, electron cloud density is mainly distributed in conjugated phenyl part in HOMO of excited enol tautomer of **C7**, while it is primarily located at *o*-hydroxy-phenyl-imino part in LUMO of excited enol form. This means that proton transfer segment can be more reactive in LUMO of excited enol form of **C7**. Thus, electron cloud density distribution in frontier orbitals of excited enol tautomers suggests that **C7** is more able to process internal proton transfer in excited state than **C1**.

We further analyze molecular geometry optimization parameters of enol and keto tautomers and transition state (TS) forms of the target dyes are shown in **Figure 7** (also see **Figure S6**). First, it is found that transition state of phototautomerization of **C1** can not be acquired, which indicates that TS form is unstable in excited state of **C1**. This means that intramolecular proton transfer in excited state of **C1** could be hard. While the presence of stable transition state of enol-keto phototautomerization of **C7** means a large possibility of ESIPT.

Table 4 shows that the distances of O-H and N-H in TS forms are between those of tautomers enol and keto in S_0 and S_1 states (such as in S_1 of **C7**, O-H, E, 0.944 Å, TS, 1.179 Å, K, 1.856 Å, **Table 4**). The smallest O-N distance in TS forms in the ground and excited states respectively suggests that there is the strongest hydrogen bond in TS (such as in S_1 of **C7**, O-N, E, 2.826 Å, TS, 2.401 Å, K, 2.673 Å). The results in turn suggest that enol-keto tautomerization in S_0 and S_1 is required to go through a transition state. It is noticed the distance of N-H in excited enol tautomer of **C1** is longer than that of **C7** (2.495 Å for **C1**, 2.084 Å for **C7**), indicating a longer internal proton transfer tunnel in **C1**.

As shown in **Table 5**, dihedral angles of ∠COHN and ∠CCNC in *o*-hydroxy-phenyl-imino part of the target dyes are given. A large variation of dihedral angle of∠COHN from S_0 to S_1 in

enol form of **C1 (**$\angle C_1$-O_1-H_1-N_1, enol form, 5.301˚ in S_0 to 1.737˚ in S_1**)** reflects that phenolic hydroxy group becomes loose in S_1, which facilitates proton transfer occurrence. In addition, the smaller dihedral angle in TS form of **C7** shows the greater coplanarity in *o*-hydoxy-phenyl-imino part in TS in excited state ($\angle C_1$-O_1-H_1-N_1, TS form, 1.111˚ in S_0 to -0.009˚ in S_1), which is favorable for internal proton transfer. While the corresponding dihedral angle of $\angle$COHN in enol form of **C1** are lower in S_1 **(**$\angle C_1$-O_1-H_1-N_1, enol form, 5.301˚ in S_0 to 1.737˚ in S_1**)**, implying that phenolic hydroxy group tends to be tight in excited state. Hence, it is more difficult for **C1** to undergo intramolecular proton transfer in excited state comparing to **C7**.

It is further found that as E of **C7** is excited to E^*, oxygen atom of phenolic group shows a decrease in negative charge, but hydrogen atom of phenolic group presents a decrease in positive charge (**Table 6**, -0.672 e to -0.651 e for O atom, 0.403 e to 0.384 e for H atom). In contrast, a reversible tendency is shown during E to E^* transition of **C1** (-0.659 e to -0.666 e for O atom, 0.349 e to 0.369 e for H atom)**.** The results indicate that phenolic group in **C7** is more acidity and more active in excited state, and thus proton in phenolic group in **C7** is more reactive accordingly. It is also found that **C7** shows a quite lower dipole moment change during tautomerization in ground and excited states than **C1** (**Table 7**, such as enol form of **C1**, 3.235 D to 5.710 D; such as enol form of **C7**, 2.660 D to 5.015 D). This means a smaller energy to achieve such a dipole moment change for **C7** comparing to **C1**.

3.6.2. Energy barriers of enol-keto tautomerization of in S_0 and S_1 states

Plots of potential energy curves (PEC) of tautomerization in S_0 and S_1 are acquired by specifying a reaction coordinate of the distance from O atom to H atom. **Figure 8** suggests that

there is an absence of TS form in excited state of **C1** and K form is more unstable in excited state in **C1**. The energy of enol-keto tautomerization in excited state of **C1** keeps increasing, indicating that it is impossible for undergoing four-level cycle process ($E \rightarrow E^* \rightarrow K^* \rightarrow K \rightarrow E$). However, the energy of K form in excited state of **C7** is much lower than that of enol form, which suggests that K form is more stable in excited state of **C7**. Furthermore, there is a quite small energy barrier of E-K tautomerization in excited state of **C7** (about 6.50 kcal/mol).

As a matter of fact, the other target partners **C2**/**C8** and **C3**/**C9** show the similar contrasting molecular geometry optimization results as **C1**/**C7**. The calculated results reflect that the targets **C7**-**C9** show a greater capacity to undergo intramolecular proton transfer in excited state through a reasonable six number-membered ring transition state, while it is difficult for **C1**-**C3** to proceed enol-keto phototautomerization through a five number-membered ring transition state.

4. Conclusions

In summary, this study presents a variety of dyes that could undergo internal proton transfer in excited state through five- and six- number-membered ring transition states respectively. X-ray single crystal diffraction and ^{1}H-NMR spectroscopy show that there is different strength intramolecular hydrogen bond between five number-membered ring transition states dyes and six number-membered ring ones. Based on the effect of internal hydrogen bond on UV/visible spectra, the fluorescence emission spectra demonstrate excited state intramolecular proton transfer occurred via six number-membered ring transition state. However, no solid experimental evidence suggests the occurrence of ESIPT through five number-membered ring transition states of the studied dyes. The remarkable difference in molecular geometry optimization of the studied dyes

leads to the diversities between five- and six- number-membered ring transition states for internal proton transfer in excited state. This study suggests that if we develop new dyes with ESIPT nature occurred via five number-membered ring transition states, an enhanced intramoleuclar hydrogen bond could be required.

Acknowledgements

The authors thank Chongqing Natural Science Foundation CSTC2012jjB50007 and CSTC2010BB0216 greatly. H. Li appreciates the Postdoctoral Science Foundation of China for financial supporting (Grant No. 22012T50762 & 2011M501388).

Supplementary materials

The ^{1}H-NMR spectra of the major products of **C4** and **C10** are included in ***Supplementary materials***. The absorption spectra and steady and transient fluorescence emission spectra of the studied dyes in various media are also provided in ***Supplementary materials***. The optimized geometries of enol, TS and keto forms in the ground state of the target dyes, the spectral parameters of the dyes and the crystallographic data are further contained in ***Supplementary materials***. The document is available free of charge from the website of this journal.

The supplementary crystallographic data for this work can be also found in files CCDC numbered by 1502866 and 1518272, which are available http://www.ccdc.cam.ac.uk/conts/retrieving.html or from the Cambridge crystallographic data center, 12, Union Road, Cambridge CB2 1EZ, UK; fax: 44-1223-336033.

References

[1] A. S. Klymchenko, V. V. Shvadchak, D. A. Yushchenko, N. Jain, Y. Mély, Excited-state intramolecular proton transfer distinguishes microenvironments in single-and double-stranded DNA, J. Phys. Chem. B 112 (2008) 12050-12055.

[2] K. C. Tang, M. J. Chang, T. Y. Lin, H. A. Pan, T. C. Fang, K. Y. Chen, W. Y. Hung, Y. H. Hsu, P. T. Chou, Fine tuning the energetics of excited-state intramolecular proton transfer (ESIPT): white light generation in a single ESIPT system, J. Am. Chem. Soc. 133 (2011) 17738-17745.

[3] A. P. Demchenko, K. C. Tang, P. T. Chou, Excited-state proton coupled charge transfer modulated by molecular structure and media polarization, Chem. Soc. Rev. 42 (2013) 1379-1408.

[4] D. K. Rana, S. Dhar, A. Sarkar, S. C. Bhattacharya, Dual intramolecular hydrogen bond as a switch for inducing ground and excited state intramolecular double proton transfer in doxorubicin: an excitation wavelength dependence study, J. Phys. Chem. A 115 (2011) 9169-9179.

[5] M. Jadhao, O. R. Meitei, R. Joshi, H. Kumar, C. Das, S. K. Ghosh, ESIPT reaction of potential bioactive heterocyclic Schiff base: Atomic visualization coupled with in vitro spectroscopy, J. Photochem. Photobiol. A: Chem. 326 (2016) 41-49.

[6] R. Hu, J. Fang, D. Hu, S. Wang, S. Li, Y. Li, G. Yang, A rapid aqueous fluoride ion sensor with dual output modes, Angew. Chem. Int. Ed. 49 (2010) 4915-4918.

[7] A. I. Ciuciu, K. Skonieczny, D. Koszelewski, D. T. Gryko, L. Flamigni, Dynamics of Intramolecular Excited State Proton Transfer in Emission Tunable, Highly Luminescent Imidazole Derivatives, J. Phys. Chem.C 117 (2013) 791-803.

[8] R. Daengngern, N. Kungwan, Dynamics simulations of photoinduced proton transfer reactions of 2-(2′-hydroxyphenyl)benzoxazole in the gas phase and its hydrated clusters, Chem. Phys. Lett. 609 (2014) 147-154.

[9] (a) X. D. Jin, C. Z. Liu, X. M. Wang, H. Huang, X. Q. Zhang, H. J. Zhu, A flavone-based ESIPT fluorescent sensor for detection of N_2H_4 in aqueous solution and gas state and its imaging in living cells, Sens. Actuators B 216 (2015) 141-149. (b) X. D. Jin, X. L. Sun, X. Y. Di, X. Q. Zhang, H. Huang, J. N. Liu, P. W. Ji, H. J. Zhu, Novel fluorescent ESIPT probe based on flavone for nitroxyl in aqueous solution and serum, Sens. Actuators B 224 (2016) 209-216.

[10] Y. Qian, S. Y. Li, Q. Wang, X. H. Sheng, S. K. Wu, S. Q. Wang, J. Li, G. Q. Yang, A nonpolymeric highly emissive ESIPT organogelator with neither dendritic structures nor long alkyl/alkoxy chains, Soft Mater. 8 (2012) 757-764.

[11] Z. Y. Zhang, Y. H. Hsu, Y. A. Chen, C. L. Chen, T. C. Lin, J. Y. Shen, P. T. Chou, New six-and seven-membered ring pyrrole–pyridine hydrogen bond systems undergoing excited-state intramolecular proton transfer, Chem. Commu. 50(95) (2014) 15026-15029.

[12] (a) Y. L. Gong, Y. Lu, H. Y. Ma, G. Ding, S. T. Zhang, Z. P. Luo, H. R. Li, F. Gao, Efficient enhancement of internal proton transfer of branched π-extended organic chromophore under one-photon and near-infrared two-photon irradiation, Chem. Phys. Lett. 619 (2015) 201-207. (b) G. Ding, Y. Lu, Y. L. Gong, L. Ma, Z. P. Luo, S. T. Zhang, F. Gao, H. R. Li, New AB2 type two-photon absorption dyes for well-separated dual-emission: molecular preorganization based approach to photophysical properties, Tetrahedron 72 (2016) 3040-3056.

[13] (a) J. Zhou, R. Y. Shi, J. X. Liu, R. Wang, Y. F. Xu, X. H. Qian, An ESIPT-based fluorescent

probe for sensitive detection of hydrazine in aqueous solution, Org. & Biomol. Chem. 13 (2015) 5344-5348. (b) S. Goswami, A. Manna, S. Paul, A.K. Das, P.K. Nandi, A.K. Maity, P. Saha, A turn on ESIPT probe for rapid and ratiometric fluorogenic detection of homocysteine and cysteine in water with live cell-imaging, Tetrahedron Lett., 55(2) (2014) 490-494.

[14] (a) W. S. Yu, C. C. Cheng, Y. M. Cheng, P. C. Wu, Y. H. Song, Y. Chi, P. T. Chou, Excited-state intramolecular proton transfer in five-membered hydrogen-bonding systems: 2-pyridyl pyrazoles, J. Am. Chem. Soc. 125 (2003) 10800-10801. (b) R. B. Singh, S. Mahanta, N. Guchhait, Photophysical properties of 1-acetoxy-8-hydroxy-1, 4, 4a, 9a - tetrahydroanthraquinone: Evidence for excited state proton transfer reaction, Chem. Phys. 331 (2007)189-199.

[15] A. I. Ciuciu, K. Skonieczny, D. Koszelewski, D. T. Gryko, L. J. Flamigni, Dynamics of Intramolecular Excited State Proton Transfer in Emission Tunable, Highly Luminescent Imidazole Derivatives, J. Phys. Chem. C, 117 (2013) 791-803.

[16] J. Jankowska, M. F. Rode, J. Sadlej, A. L. Sobolewski, Photophysics of Schiff bases: theoretical study of salicylidene methylamine, ChemphysChem. 13 (2012) 4287-4294.

[17] D. D. Perrin, W. L. F. Armarego, D. R. Perrin, Purification of laboratory chemicals; Pergamon: New York, NY, 1966.

[18] C. M. da Silva, D. L. da Silva, C. V. Martins, M. A. de Resende, E. S. Dias, T. F. Magalhães, L. P. Rodrigues, A. A. Sabino, R. B. Alves, Â. de Fátima, Synthesis of aryl aldimines and their activity against fungi of clinical interest, Chem. Biol. Drug Des. 78 (2011) 810-815.

[19] (a) L. Ilies, Y. Sato, C. Mitsui, H. Tsuji. E. Nakamura, Modular Synthesis of Polybenzo [b] silole Compounds for Hole−Blocking Material in Phosphorescent Organic Light Emitting

Diodes, Chem. Asian J. 5 (2010) 1376-1381. (b) G. W. Men, C. R. Chen, S. T. Zhang, C. S. Liang, Y. Wang, M. Y. Deng, H. X. Shang, B.Yang, S. M. Jiang, A real-time fluorescent sensor specific to Mg^{2+}: crystallographic evidence, DFT calculation and its use for quantitative determination of magnesium in drinking water, Dalton T. 44 (2015) 2755-2762.

[20] (a) M. Z. Zgiershi, A. J. Grabowska, Theoretical approach to photochromism of aromatic Schiff bases: A minimal chromophore salicylidene methylamine, J. Chem. Phys. 113 (2000) 7845-7852. (b) P. Yi, Y. H. Liang, C. Z. Cao, Intramolecular proton or hydrogen-atom transfer in the ground-and excited-states of 2-hydroxybenzophenone: a theoretical study, Chem. Phys. 315 (2005) 297-302.

[21] (a) Y. H. Liang, P. G. Yi, Theoretical studies on structure, energetic and intramolecular proton transfer of alkannin, Chem. Phys. Lett. 438 (2007) 173-177. (b) Z. N. Yang, S. Y. Yang, J. P. Zhang, Ground-and excited-state proton transfer and rotamerism in 2-(2-Hydroxyphenyl)-5-phenyl-1, 3, 4-oxadiazole and its O/"NH or S"-substituted derivatives, J. Phys. Chem. A 111 (2007) 6354-6360.

[22] (a) E. Bardez, I. Devol, B. Larrey, B. Valeur, Excited-State Processes in 8-Hydroxyquinoline: Photoinduced Tautomerization and Solvation Effects, J. Phys. Chem. B 101 (1997) 7786-7793. (b) W. S. Yu, C. C. Cheng, Y. M. Cheng, P. C. Wu, Y. H. Song, Y. Chi, P. T. Chou, J. Am. Chem. Soc. 125 (2003) 10800-100801.

[23] (a) J. Casanovas, A. M. Namba, S. León, G. L. Aquino, G. V. José da Silva, C. Alemán, Calculated and experimental NMR chemical shifts of p-menthane-3,9-diols. A combination of molecular dynamics and quantum mechanics to determine the structure and the solvent effects, J. Org. Chem. 66 (2001) 3775-3782. (b) G. Wagner, A. Pardi, K. Wuethrich, Hydrogen bond

length and proton NMR chemical shifts in proteins, J. Am. Chem. Soc. 105 (1983) 5948-5949.

[24] R. Casadesús, M. Moreno, J. M. Lluch, Theoretical study of the photoinduced intramolecular proton transfer and rotational processes in 2-(2′ hydroxyphenyl)-4-methyloxazole in gas phase and embedded in β-cyclodextrin, J. Photochem. Photobiol. A: Chem. 173 (2005) 365-374.

[25] (a) G. A. Parada, T. F. Markle, S. D. Glover, L. Hammarström, S. Ott, B. Zietz, Control over Excited State Intramolecular Proton Transfer and Photoinduced Tautomerization: Influence of the Hydrogen‐Bond Geometry, Chem.-A Eur. J. 21 (2015) 6362-6366. (b) H. W. Tseng, J. Q. Liu, Y. A. Chen, C. M. Chao, K. M. Liu, C. L. Chen, T. C. Lin, Harnessing excited-state intramolecular proton-transfer reaction via a series of amino-type hydrogen-bonding molecules, J. Phys. Chem. Lett. 6 (2015) 1477-1486.

[26] M. Ziółek, J. Kubicki, A. Maciejewski, R. Naskręcki, A. Grabowska, An ultrafast excited state intramolecular proton transfer (ESPIT) and photochromism of salicylideneaniline (SA) and its “double” analogue salicylaldehyde azine (SAA), A controversial case, Phys. Chem. Chem. Phys. 6(19) (2004) 4682-4689.

[27] M. Sliwa, N. Mouton, C. Ruckebusch, L. Poisson, A. Idrissi, S. Aloïse, S. Aloïse, L. Potier, J. Dubois, O. Poizata, G. Buntinx, Investigation of ultrafast photoinduced processes for salicylidene aniline in solution and gas phase: toward a general photo-dynamical scheme, Photoch. Photobio. Sci. 9(5) (2010) 661-669.

[28] J. B. Birks, Photophysics of Aromatic Molecules ~Wiley-Interscience, New York, 1970.

[29] R. S. Becker, Theory and Interpretation of Fluorescence and Phosphorescence ~Wiley-Interscience, New York, 1969.

[30] J. R. Lakowicz, Principles of Fluorescence Spectroscopy ~Plenum, New York, 1983.

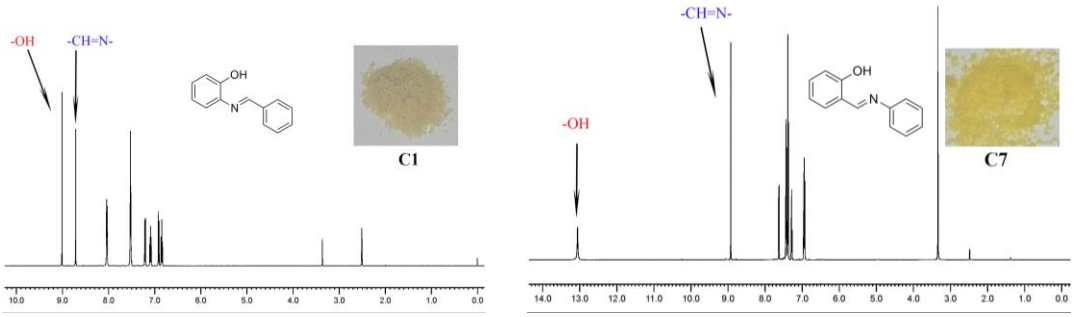

Figure 1 ^{1}H-NMR spectra of **C1** and **C7** in DMSO-d_6

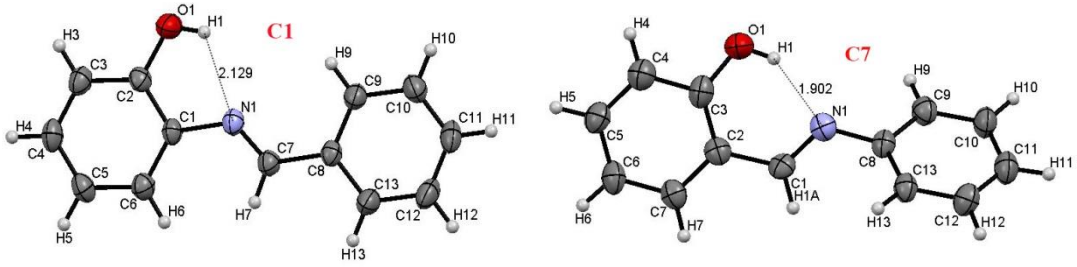

Figure 2 ORTEP drawing of **C1** and **C7** with 30% possibility of thermal ellipsoids

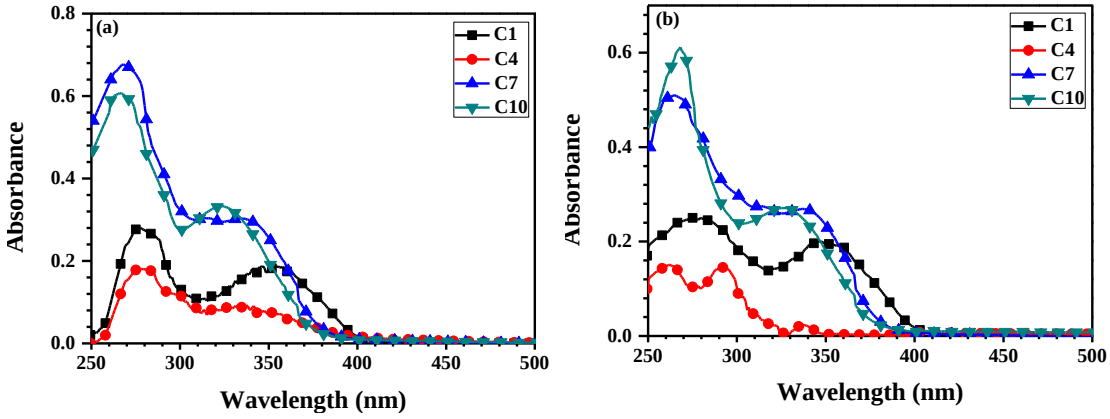

Figure 3 UV/visible absorption spectra of **C1**/**C4** and **C7**/**C10** in 1,4-dioxane (a) and in DMF (b), the concentration is 2×10^{-5} mol/L

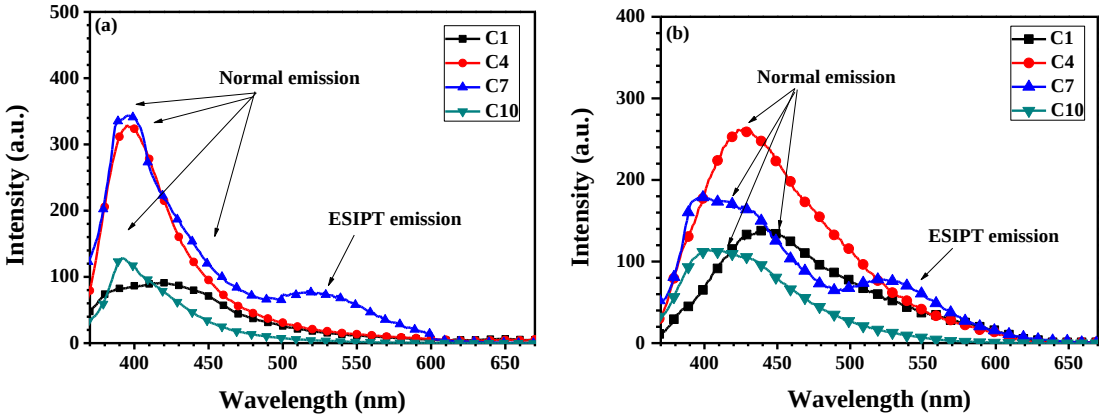

Figure 4 Steady emission spectra of **C1/C4** and **C7/C10** in 1,4-dioxane (a) and in DMF (b), the concentration is 5×10^{-6} mol/L, Excitation at 350 nm

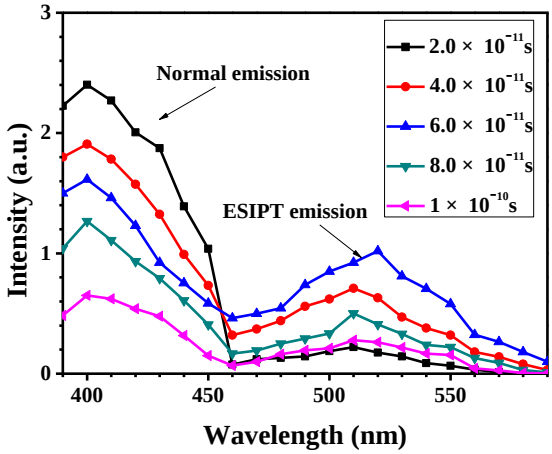

Figure 5 Time-resolved fluorescence spectra of **C8** in 1,4-dioxane, the concentration is 5×10^{-5} mol/L

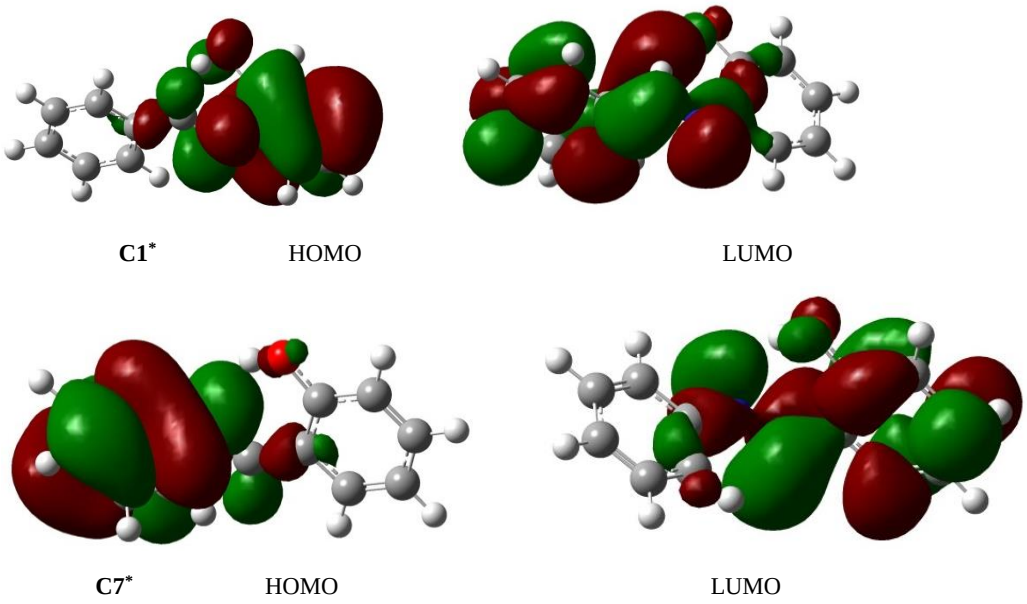

Figure 6 Frontier orbitals of enol form in the excited states of enol tautomers of **C1** and **C7**

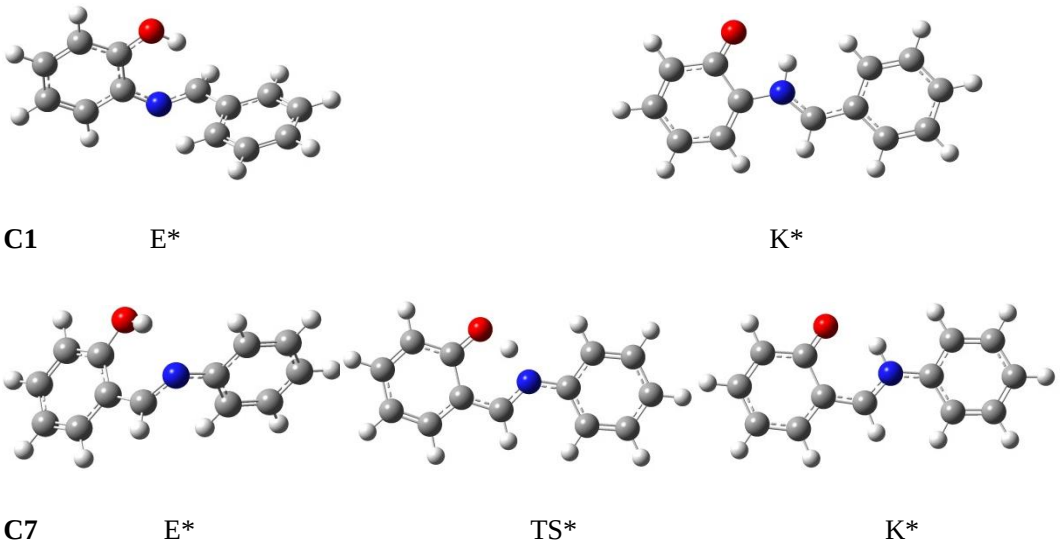

Figure 7 Optimized geometries of enol, TS, and keto forms of **C1** and **C7** in the excited state by Gaussian 09 program package

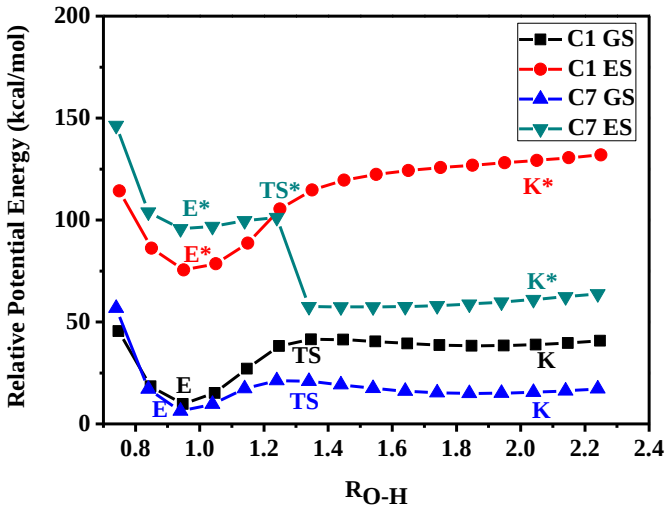

Figure 8 Proton transfer reaction potential energy curves relaxed along the O-H distance at ground and the first excited single state for **C1** and **C7**

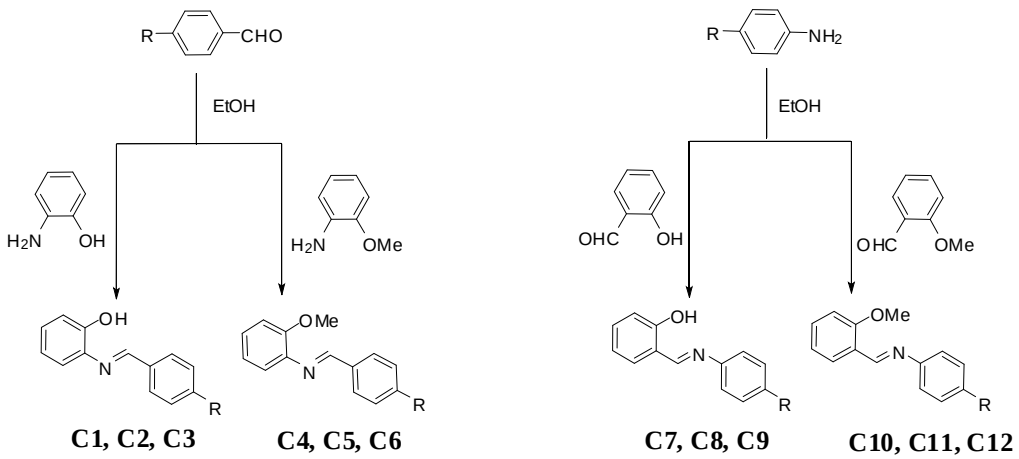

C1, C4, C7, C10, R= -H; C2, C5, C8, C11, R= -OCH_3; C3, C6, C9,C12, R= -CN

Scheme 1 Synthesis of the target molecules studied in this work

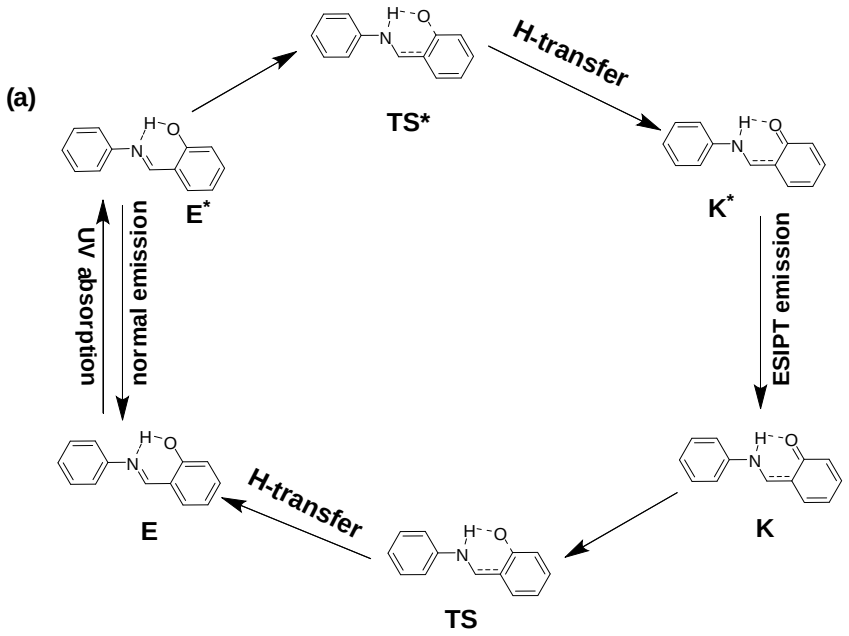

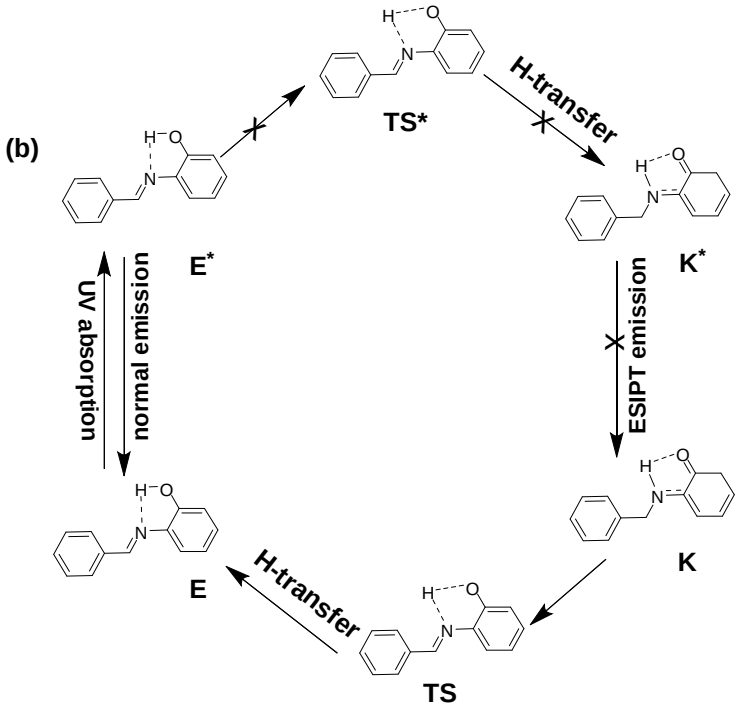

Scheme 2 A four-level cycle of enol-keto phototautomerization during internal proton transfer in excited states of **C7** (a) and **C4** (b) through different number-membered ring transition states

Table 1 UV/visible pectral parameters of **C1**/**C4** and **C7**/**C10** in various solvents, $\lambda_{a,max}$, the absorption maximum (nm), ε_{max}, the maximal molar extinction coefficient ($10^5 \bullet cm^{-1} \bullet mol^{-1} \bullet L$)

Solvents	C1		C4		C7		C10	
	$\lambda_{a,max}$	ε_{max}	$\lambda_{a,max}$	ε_{max}	$\lambda_{a,max}$	ε_{max}	$\lambda_{a,max}$	ε_{max}
1,4-dioxane	353	0.0892	330	0.0538	337	0.171	321	0.181
THF	350	0.113	337	0.0405	332	0.142	322	0.195
EtOAc	355	0.116	339	0.0267	336	0.125	324	0.144
CH_2Cl_2	351	0.114	337	0.0562	336	0.122	324	0.104
$CHCl_3$	353	0.0981	331	0.0303	333	0.143	325	0.152
MeCN	344	0.0563	338	0.0314	331	0.162	325	0.175
DMSO	346	0.0276	332	0.0295	336	0.204	321	0.191
DMF	348	0.0971	336	0.0121	338	0.149	325	0.142
Ethanol	342	0.0713	336	0.0341	335	0.127	326	0.163

Table 2 Steady emission spectral parameters of **C1**/**C4** and **C7**/**C10** in various solvents, $\lambda_{f,max}$: the emission maximum (nm), Φ: the fluorescence quantum yield

Solvents	**C1**		**C4**		**C7**		**C10**	
	$\lambda_{f,max}$	Φ	$\lambda_{f,max}$	Φ	$\lambda_{f,max}$	Φ	$\lambda_{f,max}$	Φ
1,4-dioxane	428	0.147	408	0.121	401, 516	0.0529	401	0.0391
THF	431	0.171	421	0.141	403, 516	0.0445	407	0.0470
EtOAc	427	0.113	421	0.132	404, 513	0.0602	403	0.0262
CH_2Cl_2	433	0.128	422	0.128	405, 517	0.0851	402	0.0770
$CHCl_3$	431	0.164	424	0.171	398, 514	0.103	399	0.109
MeCN	432	0.131	420	0.182	408, 513	0.0292	406	0.119
DMSO	435	0.158	424	0.177	404, 519	0.0694	404	0.0512
DMF	438	0.189	427	0.150	409, 517	0.122	405	0.163
Ethanol	436	0.169	423	0.176	404, 509	0.0751	403	0.132

Table 3 Radiative transition constants (s^{-1}) of the tautomers enol and keto decay in excited state of **C2**/**C5** and **C8**/**C11**

Dyes		**Solvents**	
		1,4-Dioxane	DMF
C2	$\Phi_{f\,(enol)}$	0.125	0.132
	$\tau_{f\,(enol)} \times 10^{-11}$(s)	2.63	2.75
	$k_{r\,(enol)} \times 10^{10}(s^{-1})$	0.475	0.447
	$k_{nr(enol)} \times 10^{11}\,(s^{-1})$	0.333	0.316
C5	$\Phi_{f\,(enol)}$	0.123	0.146
	$\tau_{f\,(enol)} \times 10^{-11}$(s)	2.34	2.28
	$k_{r\,(enol)} \times 10^{10}(s^{-1})$	0.525	0.640
	$k_{nr(enol)} \times 10^{11}\,(s^{-1})$	0.375	0.374
C8	$\Phi_{f\,(enol)}$	0.0796	0.0992
	$\tau_{f\,(enol)} \times 10^{-11}$(s)	2.26	1.98
	$k_{r\,(enol)} \times 10^{10}(s^{-1})$	0.352	0.501
	$k_{nr(enol)} \times 10^{11}\,(s^{-1})$	0.407	0.455
	$\Phi_{f\,(keto)}$	0.0332	0.0160
	$\tau_{f(keto)} \times 10^{-12}$(s)	1.78	1.37
	$k_{r\,(keto)} \times 10^{11}(s^{-1})$	0.186	0.117
	$k_{nr(enol)} \times 10^{12}\,(s^{-1})$	0.543	0.718
C11	$\Phi_{f\,(enol)}$	0.116	0.103
	$\tau_{f\,(enol)} \times 10^{-11}$(s)	2.07	2.11
	$k_{r\,(enol)} \times 10^{10}(s^{-1})$	0.560	0.488
	$k_{nr(enol)} \times 10^{11}\,(s^{-1})$	0.427	0.425

Table 4 The most important bond lengths (Å) associated with ESIPT: ground state at HF level and excited state at CIS level

Structural parameters		Ground state			Excited state		
		E	TS	K	E*	TS*	K*
C1	R_{O-H}	0.947	1.387	1.884	0.950		2.026
	R_{N-H}	2.162	1.152	1.019	2.495		1.001
	R_{O-N}	2.737	2.346	2.539	2.924		2.565
C7	R_{O-H}	0.954	1.272	1.859	0.944	1.179	1.856
	R_{N-H}	1.889	1.184	1.005	2.084	1.280	1.008
	R_{O-N}	2.712	2.384	2.658	2.826	2.401	2.673

Table 5 The most important dihedral angle (°): ground state at HF level and excited state at CIS level

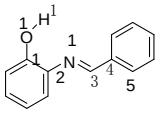

C1

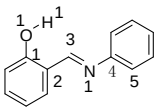

C7

Structural Parameters		Ground state			Excited state		
		E	TS	K	E*	TS*	K*
C1	$\angle C_1\text{-}O_1\text{-}H_1\text{-}N_1$	5.301	-0.003	0.004	1.737		0.000
	$\angle N_1\text{-}C_3\text{-}C_4\text{-}C_5$	5.645	-0.012	-0.027	-10.175		-0.002
	$\angle C_1\text{-}C_2\text{-}N_1\text{-}C_3$	-28.813	-0.022	0.002	0.018		0.004
	$\angle C_2\text{-}N_1\text{-}C_3\text{-}C_4$	-1.417	-0.002	-0.003	80.201		-0.002
C7	$\angle C_1\text{-}O_1\text{-}H_1\text{-}N_1$	-0.021	1.111	-0.024	35.382	-0.009	-0.007
	$\angle C_3\text{-}N_1\text{-}C_4\text{-}C_5$	44.122	-0.464	-0.002	0.562	-0.001	0.007
	$\angle C_1\text{-}C_2\text{-}C_3\text{-}N_1$	0.756	34.639	0.011	-7.648	0.007	0.000
	$\angle C_2\text{-}C_3\text{-}N_1\text{-}C_4$	-1.459	-0.791	-0.005	-86.287	0.010	-0.003

Table 6 Mulliken net atomic charges (e) of the key atoms of **C1** and **C7**

Mulliken Charge		**E**			
		C	O	H	N
Ground State	**C1**	0.384	-0.659	0.349	-0.626
	C7	0.429	-0.672	0.403	-0.680
Excited State	**C1**	0.318	-0.666	0.369	-0.670
	C7	0.446	-0.651	0.384	-0.775

Table 7 Dipole moments (D) of tautomers calculated at HF level for ground state and at CIS level for excited state to **C1** and **C7** respectively

Dipole moment	**Ground state**			**Excited state**		
	μ_E	**μ_{TS}**	**μ_K**	**μ_E**	**μ_{TS}**	**μ_K**
C1	3.235	6.691	8.027	5.710		8.552
C7	2.660	3.867	3.897	5.015	3.099	4.618